A Numerical Study of the Flow Interference between Two Circular Cylinders in Tandem by Scale-Adaptive Simulation Model

M. Grioni[1,2†], S. A. Elaskar[1,3,4], and A. E. Mirasso[2]

[1] National Scientific and Technical Research Council, CONICET, Argentina
[2] Institute of Structural Mechanics and Seismic Risk, National University of Cuyo, Mendoza, 5500, Argentina
[3] Department of Aeronautical, National University of Córdoba, Córdoba, 5000, Argentina
[4] Institute of Advanced Studies in Engineering and Technology (IDIT), CONICET - UNC, Argentina

† Corresponding Author Email: maurogrioni15@gmail.com

ABSTRACT

Unsteady simulations of the flow around two cylinders arranged in tandem are carried out using Scale-Adaptive Simulation (SAS) turbulence model for high subcritical Reynolds number (Re $= 2 \times 10^5$). Three-dimensional simulations are performed for different center-to-center distances between the cylinders (L/D varies 1.1 to 7, where D is cylinder diameter). The effects of the gaps between the cylinders are analyzed through the values of mean and fluctuating force coefficients, Strouhal number, pressure distribution, as well as through the wake flow structures behind both cylinders. The results are compared with published experimental data by different authors. The obtained results reveal good general agreement with the experimental data. Besides, to explore the effects of the interference, two tandem cylinders test are compared with a single cylinder case. The results show that this simple configuration (tandem) can strongly influence the flow pattern and forces on the cylinders. A critical nondimensional distance is obtained at L/D=3 at which two different flow patterns are identified, one pattern momentarily similar to the reattachment regime and another pattern similar to the co-shedding regime.

Keywords: SAS turbulence model; Circular cylinders in tandem arrangement; Wake interference; Vortex shedding.

NOMENCLATURE

CD	drag coefficient	U_∞	free-stream velocity
CL	lift coefficient	x, y, z	cartesian coordinates
C_P	pressure coefficient	y^+	dimensionless wall distance
CFL	Courant–Friedrichs–Lewy number		
D	cylinder diameter		
f	frequency	Δt	time step
L	center-to-center distances between the cylinders	Δx	size of control volume
		θ	angle
(L/D)c	critical distance L/D	θs	separation angle
Re	Reynolds number	θr	reattachment angle
RMS	Root Mean Square	μ	dynamic viscosity
St	Strouhal number	ρ	density
t	time		

1. INTRODUCTION

Circular cylinder is a structural component widely used in engineering. Frequently the cylinders are arranged forming groups; such is the case of groups of chimneys, aerial cables of power lines, tubes in heat exchangers, chemical reaction towers, marine platforms and submarine pipelines, storage

tanks, among others. The effect of the presence of more than one body placed within the fluid stream is called the flow interference. A type of flow interference corresponds to cylinders that are aligned one behind the other (tandem), and it is referred to as 'wake interference' by Zdravkovich (1987). Depending on the distance between the cylinders, different flow behaviors occur around both cylinders that have significant effects on the vortices detached and the resulting loads on the cylinders. The pioneering studies on the classification of the flow past two tandem cylinders were carried out by Igarashi (Igarashi 1981; Igarashi 1984) and Zdravkovich (1987). These works identified three main flow regimes in function of the cylinder distance (expressed as the ratio of center-to-center distance to cylinder diameter, L/D): (i) the single extended-body regime at small spacings L/D ($1 < L/D < 1.2 − 1.8$), where periodic von Kármán vortex shedding is observed only in the wake of the downstream cylinder; (ii) the reattachment regime at intermediate spacings L/D ($1.2 − 1.8 < L/D < 3.4−3.8$), where the shear layer separated from upstream cylinder reattach on the downstream cylinder and vortex street is formed only behind the downstream cylinder; (iii) the co-shedding regime at large non-dimensional distances L/D ($L/D > 3.4−3.8$), where vortex shedding occurs from both the cylinders with the same frequency. The appearance of each flow regime depends on the value of the Reynolds number (Zdravkovich, 1987) and the free-stream turbulence intensity (Ljungkrona *et al.,* 1991). In addition to these regimes, there is a transition between the reattachment and co-shedding regimes that occur intermittently, switching from one to the other. This behavior was called bistable flow (Igarashi, 1981), and the corresponding non-dimensional distances L/D is referred to as the critical (L/D)c.

During the last decades, several experimental studies have been carried out to investigate the flow around two cylinders in tandem, e.g., by Zdravkovich and Pridden (1977); Igarashi (1981); Zhang and Melbourne (1992); Alam *et al.* (2003); Alam (2014) and Wang *et al.* (2018). Most of the previous experiments were carried out in the range of Reynolds numbers $1 \times 10^4 < Re < 8 \times 10^4$ which correspond to subcritical flow regime for an isolate circular cylinder (Niemann and Hölscher, 1990). A comprehensive review of the experimental studies for two cylinders in tandem is given by Sumner (2010). On the other hand, a more recent approach has been to study the flow around two cylinders in a tandem configuration using numerical simulations. Some of the numerical studies of the flow around isolated tandem cylinders were carried out by Meneghini *et al.* (2001), Carmo and Meneghini (2006), Mittal *et al.* (1997), Liang *et al.* (2009), Palau-Salvador *et al.* (2008) and Kitagawa and Ohta (2008). Meneghini *et al.* (2001) used a fractional step method at Re from 100 to 200, Carmo and Meneghini (2006) utilized a spectral element method

in the Re range from 160 to 320. On the other hand, Mittal *et al.* (1997) employed a finite element formulation at Re=100 and 1000, and Liang *et al.* (2009) considered that the flow is laminar at Re=100. Palau-Salvador *et al.* (2008) and Kitagawa and Ohta (2008) used LES (Large Eddy Simulation) at Re=1500 and 2.2×10^4, respectively. However, many of the works are limited to two-dimensional (2D) simulations and are restricted to Reynolds numbers less than 1000.

The primary objective of the present work is to study using 3D fluid-dynamic computations (CFD) the flows around two stationary circular cylinders in tandem. We consider arrangements at different distances from center to center between the cylinders (L/D from 1.1 to 7) at a high subcritical Reynolds number (Re = U_∞D/υ, where U_∞ is the velocity of the free current, D is the diameter of the cylinders, and υ is the kinematic viscosity of the fluid). The used Reynolds number is 1.2×10^5, equal to the experimental study carried out by Zdravkovich and Pridden (1977). Due to the flow behavior becomes complex under tandem configuration, in this work we proposed to use the hybrid turbulence model called SAS (Scale-Adaptive Simulation) proposed by Menter *et al.* (2003). This model provides standard RANS capabilities in stable flow regions and can switch to LES-like mode in unsteady regions of the flow field but without the explicit mesh dependence in the RANS regime. We have selected the SAS model because it was used successfully to analyze a similar test case: the flow around a horizontal cylinder close a plane boundary (Grioni *et al.,* 2018). The remainder of the article is organized as follow. A brief description of the numerical methodology and mathematical formulation of the turbulence model SAS, the spatial resolution and boundary condition are presented in Section 2. Numerical results and discussions are described in Section 3. Finally, the concluding remarks are given in Section 4.

2. COMPUTATIONAL MODELING

2.1 Numerical Solver

The flow past two circular cylinders in tandem is simulated considering different distances between the cylinders L/D from 1.1 to 7. The simulations are conducted using the CFD code Ansys Fluent 15 (Ansys-Fluent, 2014), in which a finite volume method is used to solve the governing equations for incompressible turbulent flow. A Semi-Implicit Method for Pressure Linked Equations algorithm (SIMPLE) is used for the velocity-pressure coupling. Second-order schemes are used for pressure and turbulent quantities discretizations. The momentum equations are discretized with a bounded central difference scheme, while the unsteady formulation is based on a bounded second-order implicit scheme.

For simulations here performed, a structured mesh is used to discretize the computational domain. A mesh
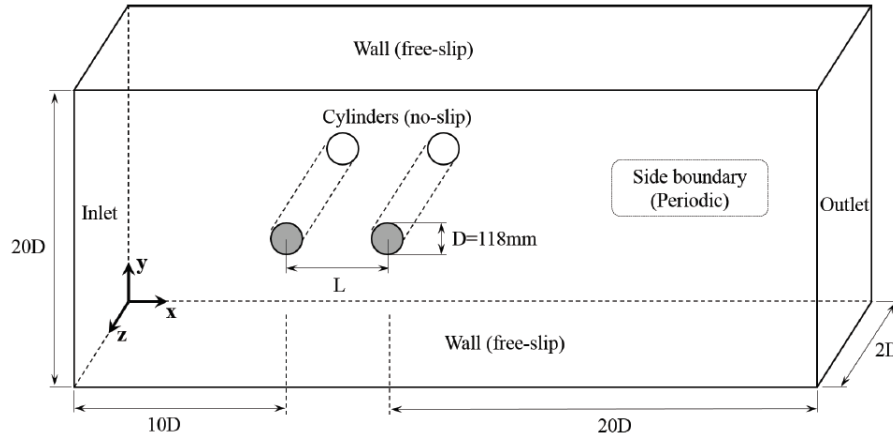
Fig. 1. Schematic diagram of the computational domain and boundary conditions.

convergence study is performed to examine the effects of mesh resolution on the results. The final implemented mesh has a suitable number of elements to achieve independent results. More details of the mesh convergence are described later. Most of the unsteady simulations in this study needed between 5 and 15 inner iterations per time step to achieve a convergent solution. The dimensionless time step $\Delta t U_\infty/D$ is set at 0.01, which ensured a value of CFL (Courant-Friedrichs-Lewy number, where CFL = $\Delta t U/\Delta x$ less than 2 for the computational domain. To ensure the time step convergence a smaller $\Delta t U_\infty/D$ of 0.0052, which give a Courant number of CFL< 1 for the entire computational domain, is computed for comparison. Further details of the time step convergence are described below. The transient simulations are executed until the stationary periodic flow pattern is achieved, and then are further continued about 20-30 vortex-shedding cycles to obtain sufficiently long time-averaged data of the flow that allow the statistical analysis.

A schematic diagram of the computational domain and used boundary conditions in this study are shown in Fig. 1. At the inlet of the domain a constant and uniform flow (15.35 m/s) with a low level of turbulence (turbulence intensity of 0.9% and turbulent viscosity ratio of unity) is imposed. At the outlet, a condition of zero-diffusion-flux for all variables in the streamwise direction is applied. This condition is referred to as the 'outflow' boundary condition in Fluent. For the upper and lower boundary of the domain, the free-slip wall is specified. For the side boundaries, periodic conditions are imposed in the spanwise direction. As concerns the surface of the cylinder, no-slip conditions are considered, i.e. the velocity at the wall is zero.

2.2 SAS Turbulence Model

The Scale-Adaptive Simulation (SAS) method can be defined as a second generation URANS (Unsteady Reynolds-Averaged Navier–Stokes), which allows the resolution of the turbulent spectrum in unstable flow conditions. The SAS concept is based on the introduction of the von Karman length-scale allowing to dynamically resolve the structures in a URANS simulation, which results in an LES-like behavior in unsteady regions of the flow field. At the same time, the model provides standard RANS capabilities in stable flow regions. The SAS method provides "LES" level off low-field capture in the unsteady areas, but the model does not contain any parameter related to the grid used for solving the transport equations. This new length scale (L_{vk}) is implemented within the model SST (Shear Stress transport) of two equations.

The SST model was formulated by Menter (1994) to combine the best characteristics of the k-ω and k-ε model, and also to lead to significant improvements in the prediction of adverse pressure gradient flows. Although the SST model has shown a good performance near the wall region, in transient flows it has the drawback of producing too large turbulent length-scales. In the SAS approach, this limitation is overcome by introducing the von Karman length-scale, which is given by;

$$L_{vk} = \kappa \sqrt{\frac{\left|\dfrac{\partial U_i}{\partial x_i}\dfrac{\partial U_j}{\partial x_i}\right|}{\left|\dfrac{\partial^2 U_i}{\partial x_j}\dfrac{\partial^2 U_j}{\partial x_i}\right|}} \tag{1}$$

where κ is the von Karman constant. The provided information by the von Karman length scale allows to preserve the SST model in steady regions and to activate the SAS capability in unsteady regions of the flow field. Based on the SST model, SAS formulation can be obtained by incorporating an additional source term (Q_{SAS}) in the transport equation for the turbulence eddy frequency (ω).

$$\frac{\partial(\rho\omega)}{\partial t} + \frac{\partial(\rho U_\infty \omega)}{\partial x_j} = \frac{\partial}{\partial x_j}\left[\left(\mu + \sigma_{\omega 3}\mu_t\right)\frac{\partial\omega}{\partial x_j}\right]$$
$$+ \alpha_3\frac{\omega}{k}\tau_{ij}\frac{\partial U_i}{\partial x_j} - \rho\beta_3\omega^2 \tag{2}$$
$$+ 2\rho(1-F_1)\sigma_{\omega 2}\frac{1}{\omega}\frac{\partial k}{\partial x_j}\frac{\partial\omega}{\partial x_j} + Q_{SAS}$$
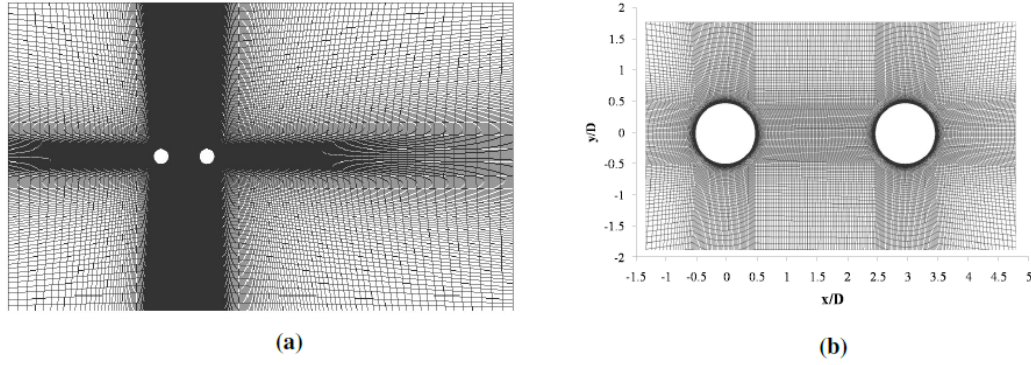
Fig. 2. Example of computational mesh for L/D=3.

with the additional source term, Q_{SAS} given as:

$$Q_{SAS} = max \left[\rho \xi_2 \kappa S^2 \left(\frac{L}{L_{vk}} \right)^2 \right.$$

$$\left. -C_{SAS} \frac{2\rho k}{\sigma_\Phi} max \left(\frac{1}{\omega} \frac{\partial \omega}{\partial x_j} \frac{\partial \omega}{\partial x_j}, \frac{1}{k^2} \frac{\partial k}{\partial x_j} \frac{\partial k}{\partial x_j} \right), 0 \right] \quad (3)$$

where the model parameters are given by $\sigma_{\omega 2} = 0.856$, $\xi_2 = 3.51$; by $\sigma_\Phi = 2/3$, $C_{SAS} = 2$ and k is the turbulent kinetic energy. F_1 is a blending function that switches smoothly between the two turbulence models. Constants with subscript 3 blend between the constants in the $k - \varepsilon$ and $k - \omega$ models (Menter, 1994).

The turbulent length scale (L) derived from the SST model is given as,

$$L = \frac{\sqrt{k}}{c_\mu^{0.25} \omega} \quad (4)$$

The turbulent eddy viscosity for SAS model is given by;

$$\mu_t = \rho \left(\sqrt{\frac{\sqrt{\frac{\beta_3 - \alpha_3}{c_\mu}}}{\kappa \eta_2}} L_{vk} \right)^2 S \quad (5)$$

where $\beta_3 = 0.075$, $c_\mu = 0.09$, $\alpha_3 = 0.55$ y $S = (2 S_{ij} S_{ij})^{1/2}$ is a scalar invariant of the strain rate tensor S_{ij} given by

$$S_{ij} = \frac{1}{2} \left(\frac{\partial U_i}{\partial x_j} + \frac{\partial U_i}{\partial x_j} \right) \quad (6)$$

2.3 Computational Mesh

Three-dimensional multi-block structured meshes created with Ansys ICEM (Ansys-ICEM, 2014) are used together with the SAS turbulence model. The mesh resolution over the cylinder is similar to the mesh used for a circular cylinder near a plane boundary by Grioni *et al.* (2018). Figure 2(a) shows an example of the two-dimensional mesh for the L/D=3, and Fig. 2(b) shows the details near the

cylinder's surface. As we can see in Fig. 2(b), a refinement is applied near the cylinders and in the space between them to capture the boundary layer on the surface of the cylinders and the flow structures between the two cylinders. The distance from the cylinders to the nearest mesh points is chosen such that the dimensionless wall distance y^+ is kept below 1, and 160 mesh points are equidistantly located around the cylinders. The three-dimensional meshes are obtained by merely extending the two-dimensional mesh in the spanwise (z) direction. The spanwise extent of the domain is set at 2 diameters (D), which is the lowest limit acceptable for turbulence resolving models (Menter *et al.,* 2003), with 20 elements equidistantly located in the z-direction. The total number of the grid elements utilized in each spacing L/D ranges from 0.91 (for L/D=1.1) to 1.31 (for L/D=7) million, as summarized in Table 1. The differences between the numbers of elements are defined to keep a similar mesh aspect ratio in the gap between the cylinders. As the downstream cylinder moves away from the upstream cylinder, the number of mesh points is increased in the distance between the cylinders.

We study 9 different meshes to investigate the flows around two stationary circular cylinders placed in tandem (one for each L/D ratio=1.1, 2, 2.5, 3, 3.5, 4, 5, 6 and 7). In addition to these 9 meshes, we use other four meshes to examine the dependency of the results with the mesh.

Table 1 Summary of mesh used to each spacing L/D

L/D	Total Elements (approx.)
1.1	$0.91 x 10^6$
2	$1.00 x 10^6$
2.5	$1.04 x 10^6$
3	$1.07 x 10^6$
3.5	$1.10 x 10^6$
4	$1.13 x 10^6$
5	$1.19 x 10^6$
6	$1.25 x 10^6$
7	$1.31 x 10^6$

2.4 Effect of Mesh and Time Resolution

We perform a mesh and time step convergence study

172

Table 2 Time average values of CD and St for both cylinders with different mesh and time resolution (L/D=5)

Cases	Mesh (x,y)	Mesh (z)	$\Delta t U_\infty/D$	CD1	CD2	St1	St2
Baseline	59496	20	0.01	0.685	0.486	0.257	0.257
Resolution(x, y)							
M1	26155	20	0.01	0.718	0.446	0.246	0.246
M2(=Baseline)	59496	20	0.01	0.685	0.486	0.257	0.257
M3	128172	20	0.01	0.696	0.484	0.257	0.257
Resolution in time							
T1(=Baseline)	59496	20	0.01	0.685	0.486	0.257	0.257
T2	59496	20	0.0052	0.699	0.457	0.250	0.250

for a tandem cylinder configuration at L/D=5. The procedure employed here is similar to that used in Grioni *et al.* (2018). Following this reference, we use similar mesh densities in the present study. First, a set of 4 meshes of different spatial resolution (in the x–y plane and also in the z–direction) are carried out to examine the effect of mesh resolution on the results. Second, two different time resolutions are compared to explore the impact of time resolution on the results. Table 2 presents a summary of overall cases, in which the mean drag coefficients and Strouhal number values are compared. The case defined as "baseline" in Table 2 indicates the adopted mesh and time resolution in the present study.

A comparison of the effects of mesh resolution in the x and y directions with 20 elements in the z-direction is shown from the cases M1, M2 (=Base-line) and M3. To obtain a constant mesh refinement ratio, in the M1 case the number of mesh points in each (x and y) direction is set in such a way that the baseline results in 50% more points than in the M1 mesh. Whereas in case of M3, the number of mesh points is increased by 50% from the baseline. From the results, the convergence may not be evident. However, the difference for CD1 and CD2 between cases M2 and M3 is smaller than those between cases M1 and M2, suggesting a certain degree of mesh convergence in the x and y directions. On the other hand, this convergence is evident for the Strouhal numbers.

To ensure the time step convergence, the case T1 (baseline) and T2 are compared. In the case of T2, the time step is reduced to half of T1, resulting in a Courant number of CFL < 1. The differences in the obtained results between the cases T1 and T2 are found to be very small, as shown in Table 2.

3. RESULTS AND DISCUSSION

The unsteady flow past two cylinders in tandem is simulated numerically using Scale-Adaptive Simulation (SAS) turbulence model for a Reynolds number of 1.2×10^5 . To identify the wake interference effects due to the proximity between the cylinders, we study several tests for L/D between 1.1 and 7. We present the results of fluid forces exerted on both cylinders through the mean and RMS (Root-Mean-Square) values, the Strouhal number, the pressure distribution, as well as the wake flow structures behind the cylinders. The present results are compared to the previously published studies of two cylinders in tandem at comparable Re number. Also, to understand the interference effects, two tandem cylinders results are compared with those calculated for one cylinder tests. The results obtained for the single cylinder simulation are detailed in Appendix A. From now on the numbered index 1 refers to the upstream cylinder, and numbered index 2 refers to the downstream cylinder.

3.1 Drag Force and Lift Force

The influence of the ratio L/D on the forces acting on the two cylinders in tandem is investigated through the time histories of the lift (CL) and drag (CD) coefficients, the mean drag coefficient and the magnitude of the fluctuating drag and lift coefficients represented by its root-mean-square (RMS) value, CDRMS and CLRMS, respectively. The drag and lift coefficients are defined as CD = $FD/(0.5\rho U_\infty^2 A)$ where FD is the drag force exerted on the cylinder, and A is the projected area of the cylinder; CL = $FL/(0.5\rho U_\infty^2 A)$, where FL is the cylinder lift force.

The time histories of the force coefficients (CL, CD) of both the upstream and the downstream cylinder for the nondimensional time range $tU_\infty/D = 105 - 205$ are shown in Fig. 3. These 100 nondimensional time units corresponds to about 20-30 vortex-shedding cycles to obtain reliable statistical information. The dotted line represents the CL coefficients and the solid one the CD coefficient. For L/D < 3 the fluctuating drag and lift coefficients for the upstream and downstream cylinder are smaller than those for a single cylinder, which implies that the interference effects are present. This phenomenon can be explained because no vortices are shed from the upstream cylinder and on the other hand, the vortex structure was not clearly formed behind the downstream cylinder. Additionally, for L/D < 3 the figures show that fluctuation amplitude of CL and CD for both cylinders decreases when the spacing between the cylinders increase, up to for L/D=2.5 the fluctuation of CL and CD is almost negligible.
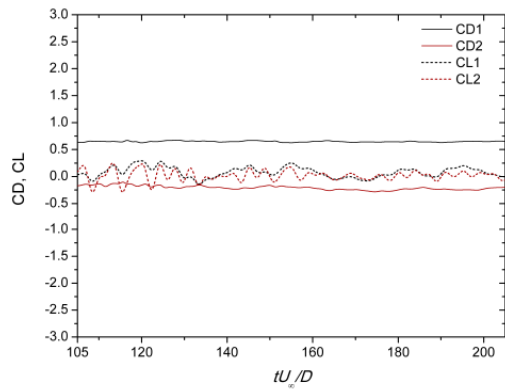
(a)
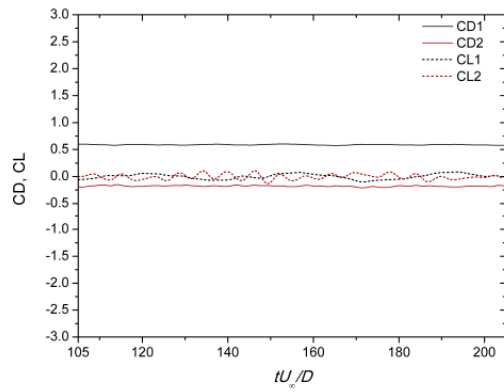
(b)
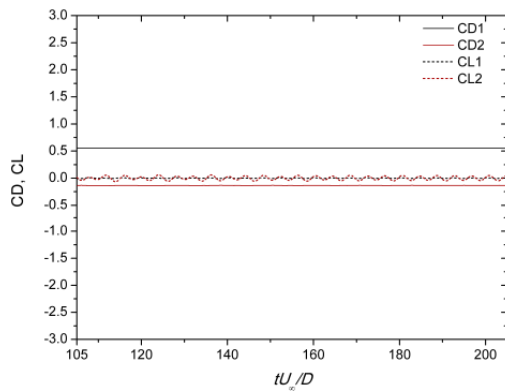
(c)
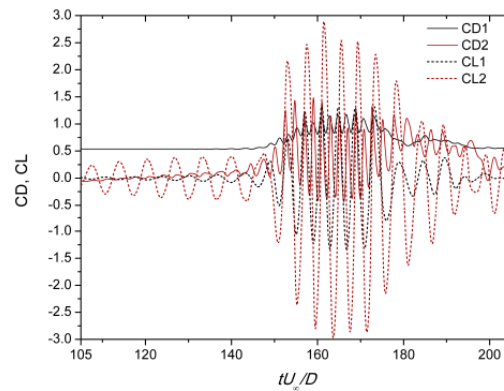
(d)
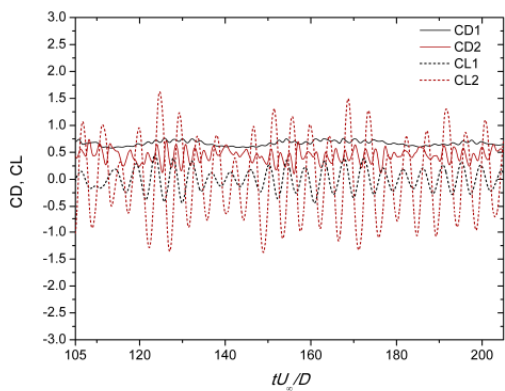
(e)
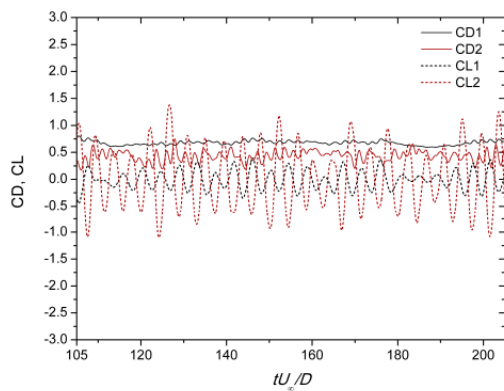
(f)
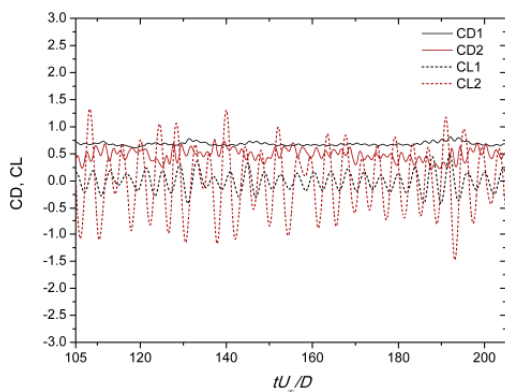
(g)
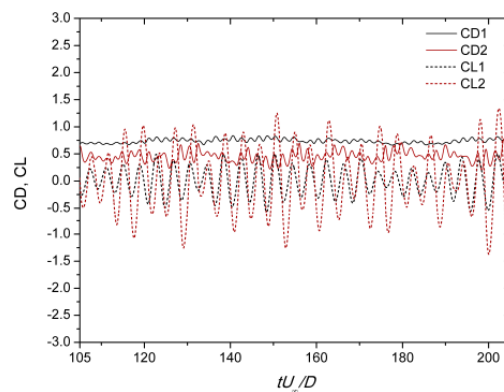
(h)
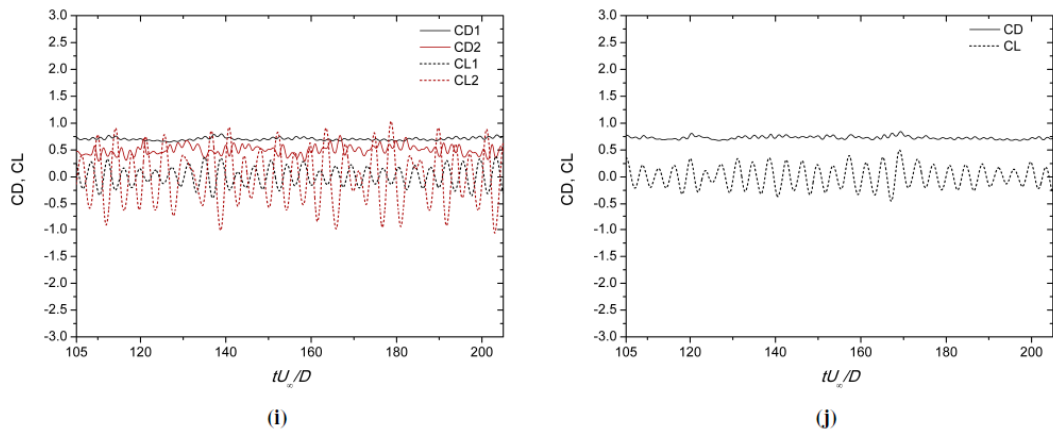
Fig. 3. Time histories of CD (solid line) and CL (dashed line) of both upstream and downstream cylinders:(a) L/D=1.1, (b) L/D=2, (c) L/D=2.5, (d) L/D=3, (e) L/D=3.5, (f) L/D=4, (g) L/D=5, (h) L/D=6, (i) L/D=7, (j) Single cylinder.

For L/D=3, the figure shows two different flow patterns. In the time range of 105−145, the fluctuating drag and lift coefficients form one pattern momentarily similar to L/D < 3, meanwhile in the time range of 145 − 205 appear another pattern, which is similar to the flow behavior for L/D > 3. This behavior indicates that the nondimensional distance L/D=3 define a transition region and the value of the critical spacing (L/D)c. This transitional behavior is consistent with the identified by Igarashi (1981), who called this a bistable flow.

For L/D > 3 the figures show that the fluctuation of CL and CD have different behavior. It can be noted that the fluctuating CL and CD for the upstream cylinder tend towards that of a single cylinder, whereas the fluctuation amplitude of CL and CD on the downstream cylinder is larger than on the upstream cylinder. Also, it can be observed that the frequency of CL fluctuation for both cylinders is resembled, suggesting that both cylinders undergo vortex shedding at the same frequency. The details of the vortex shedding will be further described in Section 3.3.

The mean drag coefficients of both the upstream and the downstream cylinders as a function of L/D are shown in Fig. 4. For comparison with present results, previously published experimental data are included. Also, to explore the effect of the interference, numerical data for a single cylinder detailed in Appendix A is added.

Considering the mean CD values for the upstream cylinder (CD1), the numerical results show an underprediction compared with the experiments obtained for Biermann and Herrnstein Jr (1934) ($Re = 1.1 \times 10^5$) and Okajima (1979) ($Re = 1.7 \times 10^5$). The cause of this discrepancy in the prediction of CD1 can be explained by the angle where the flow separation occurs for the upstream cylinder. The flow behavior for this Re (high subcritical regime) is characterized by a laminar separation at an angle of $\theta_s = 70° − 80°$ from the stagnation point as shown in Fig. 9(a) (experiment

results by Arie *et al.* (1983) at $Re = 1.57 \times 10^5$). However, the numerical simulation predicts the separation point at an angle of approximately $95° − 100°$ (see Fig. 9(a)), which would explain the reduction in the drag coefficient for the upstream cylinder. This conclusion is also confirmed recently by Rajani *et al.* (2012) and Dobrucali and Kinaci (2017), who conducted URANS simulations of a circular cylinder in free-stream using SST turbulence model. An interesting observation to note is that a similar trend is observed when compared with the experimental data, i.e., a slow decrease in CD1 with increasing L/D until a minimum and then jumps to higher values close to the value for a single cylinder.

On the other hand, the mean drag coefficient for the downstream cylinder (CD2) mostly agrees with the experimental results. The critical spacing (L/D)c appears close to 3 when the Karman vortex shedding occurs from the upstream cylinder. This result is reasonably consistent with previous measurements by Zdravkovich and Pridden (1977) and Okajima (1979), who indicate that the critical spacing ranges from 3.5 to 3.8 diameters at a Reynolds number of 1.2×10^5, and $Re = 1.7 \times 10^5$, respectively. Kitagawa and Ohta (2008) found that the critical spacing is about L/D=3.25 through numerical simulation using standard LES turbulence model at $Re = 2.2 \times 10^4$.

Compared to the drag coefficient of a single cylinder, for L/D > 3 the upstream cylinder behave as an individual entity, i.e., for L/D > 3 the mean drag force exerted on the upstream cylinder are not affected by the presence of the downstream cylinder. On the other hand, the drag force of the downstream cylinder is less than for a single cylinder, even for L/D=7, i.e., the drag force exerted on the downstream cylinder is modified when a cylinder of equal dimension is placed forward even for L/D=7. Figure 5 shows the RMS force coefficients CLRMS and CDRMS of both cylinders as a function of L/D.
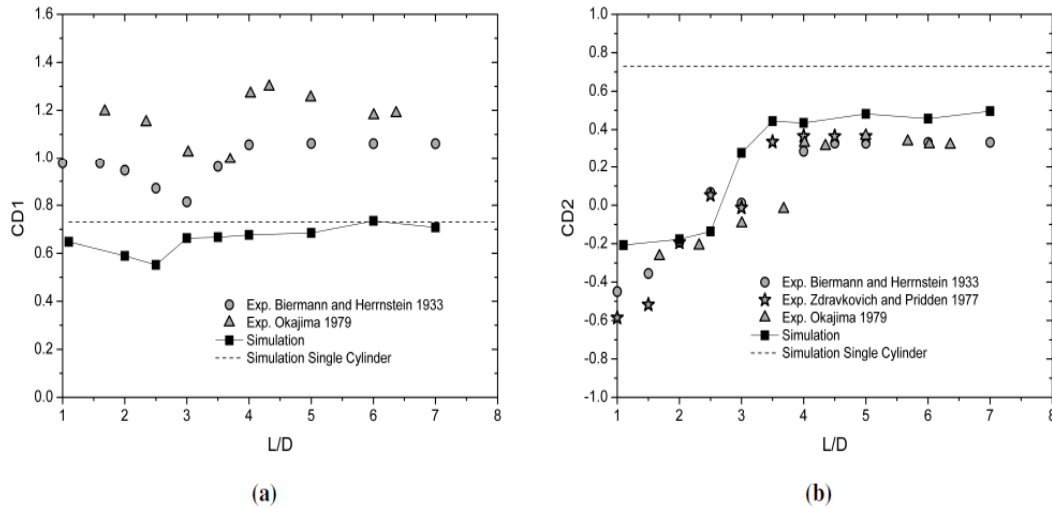
Fig. 4. Mean drag coefficients for two tandem circular cylinders as a function of spacing L/D. (a) upstream cylinder, (b) downstream cylinder.
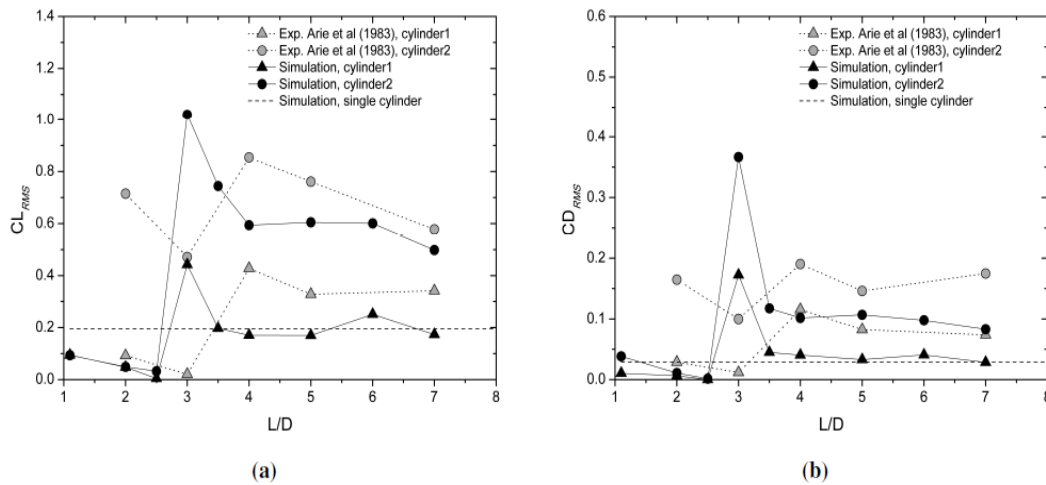
Fig. 5. RMS lift and drag coefficients of both the upstream and the downstream cylinders as a function of L/D: (a) CLRMS; (b) CDRMS.

As can be seen from the figure, the CL_{RMS} and CD_{RMS} values for the downstream cylinder are more significant than the upstream cylinder. This behavior is owing to the flow interference that the upstream cylinder produces over the downstream cylinder. A comparison with the results of the experiments conducted at similar Reynolds number ($Re = 1.57 \times 10^5$) by Arie *et al.* (1983) shows, for $L/D > 4$, a good agreement. Meanwhile for $L/D < 4$ is found a slightly larger difference with the experiments, especially in the value of L/D where appear the peak of the CL_{RMS} and CD_{RMS}, i.e., the peak values correspond to L/D=3 in this study and L/D=4 in the experimental results. A possible ex-planation for this difference can be found in the critical distance. In Arie *et al.* (1983), the critical spacing was obtained in the vicinity of L/D=4, whereas in this study the critical spacing is identified in L/D=3. Also, the RMS force coefficients obtained for a single cylinder detailed in Appendix A have been shown for comparison. A

point to note is that for large spacing ($L/D \geq 3.5$), the RMS force coefficients of the upstream cylinder tend to behave as a single cylinder meanwhile the RMS force coefficients of the downstream cylinder still show a difference with a single cylinder even at L/D=7. However, it can be observed that a certain tendency to converge is achieved when the ratio L/D increases.

3.2 Strouhal Number

The Strouhal number is defined as $St = fD/U_\infty$, where f is the vortex shedding frequency in $[s^{-1}]$ obtained from the fluctuating lift force. Figure 6 shows the variation of St number of both cylinders (St1 and St2) with different separations L/D. It can be seen that the predicted St numbers by numerical simulation agrees with the experiments of Jendrzejczyk and Chen (1985) at $Re = 1 \times 10^5$. It is also noted that, for both cylinders, the Strouhal
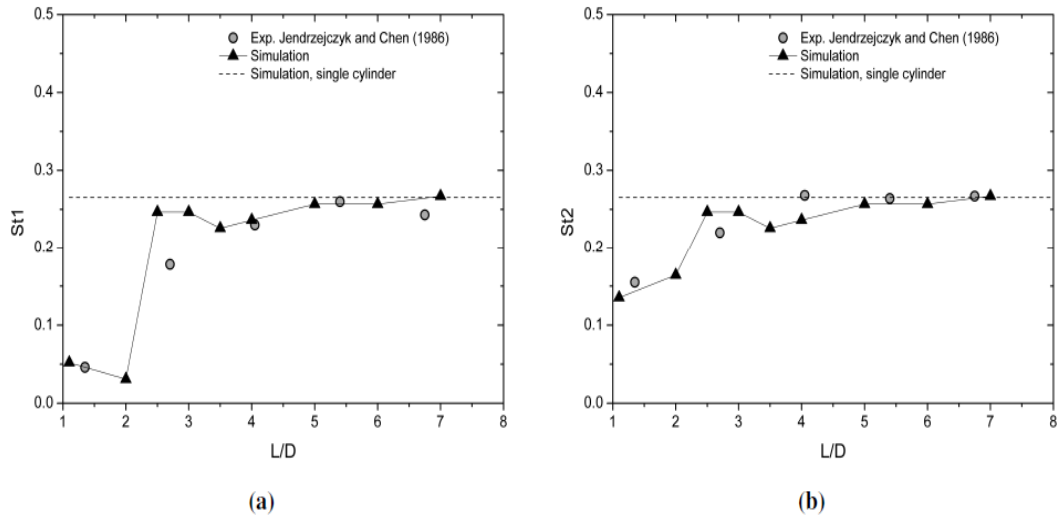
Fig. 6. Strouhal number for the upstream and downstream cylinder as a function of L/D: (a) upstream cylinder, (b) downstream cylinder.

values are very similar for L/D ≥ 2.5. This result is to be expected for L/D ≥ 3, since the vortex shedding occurs from both the cylinders. For L/D=2.5, even though the vortex shedding frequency for the upstream cylinder seems to indicate the vortex shedding formation, this behavior is not evident in Fig. 3(c). The reason for this is that the vortex formation region behind the upstream cylinder is weak which results in a fluctuation amplitude of CL well flattened for the upstream cylinder. For L/D < 2.5, a clear difference of the St values can be seen between the upstream cylinder and the downstream cylinder. This phenomenon is related to the proximity between the cylinders since alternated vortex shedding is not formed behind the upstream cylinder and this only occurs from the downstream cylinder. An interesting observation to note is that the Strouhal numbers obtained for both cylinders for L/D ≥ 5 approach the value found behind the single cylinder.

3.3 Wake Flow

The wake structure can be analyzed via the instantaneous flow fields. Figure 7 shows instantaneous contours of the spanwise vorticity, ω_z, in the mid-span sections for different ratio separation L/D.

By analyzing these figures one can see for the smallest value L/D=1.1 that the flow looks like a single body, where the region between the cylinders is stagnant and the vortex shedding forming only behind the downstream cylinder. For a further increase of the separation of the cylinders, L/D=2 and L/D=2.5, a common characteristic can be visualized. The shear layers separated from the upstream cylinder reattach to the surface of the downstream cylinder and the vortex shedding is formed only behind the downstream cylinder. Also,

it can be noticed that within the reattachment regime, certain wake symmetry in the gap can be found. For L/D=3 the two flow patterns identified above in Fig. 3(d). can be observed in the figure corresponding to L/D=3-a and L/D=3-b. In the former a quasi-stationary wake is formed in the gap between the cylinders, and in the latter, the vortex shedding is formed behind both cylinders. For L/D ≥ 3.5, a similar flow behavior can be identified, in which the vortex shedding occurs behind both cylinders. An interesting observation to note is that these vortex sheddings are generated at the same frequency, as seen in Fig. 6. These flow characteristics are consistent with the flow classification by Igarashi (1981).

In the present study, the SAS model is chosen due to this model resolves the turbulent structures. This capability was examined in the case of one cylinder near a plane boundary in Grioni *et al.* (2018). Figure 8 shows the three main flow regime through the instantaneous three-dimensional wake structures visualized with the use of iso-surfaces of the *Q*-criterion ($Q = 1/2(\Omega^2 - S^2)$), where S is the strain rate and Ω is the vorticity) colored with the turbulence viscosity ratio magnitude. The single extended-body regime is represented by L/D=1.1, the reattachment regime by L/D=2.5 and the co-shedding regime by L/D=5. It can be seen a clear difference in the three regimes, where the wake structures are strongly affected by the distance between the cylinders.

3.4 Mean Flow Characteristic

The pressure coefficient, Cp, around the mid-plane of the cylinders is defined as $Cp = (p - p_\infty)/(0.5\rho U_\infty^2)$ where p_∞ is the static pressure in the freestream and p denotes the mean pressure measured on the surface of the cylinders. Figure 9 shows the pressure coefficient distributions on the
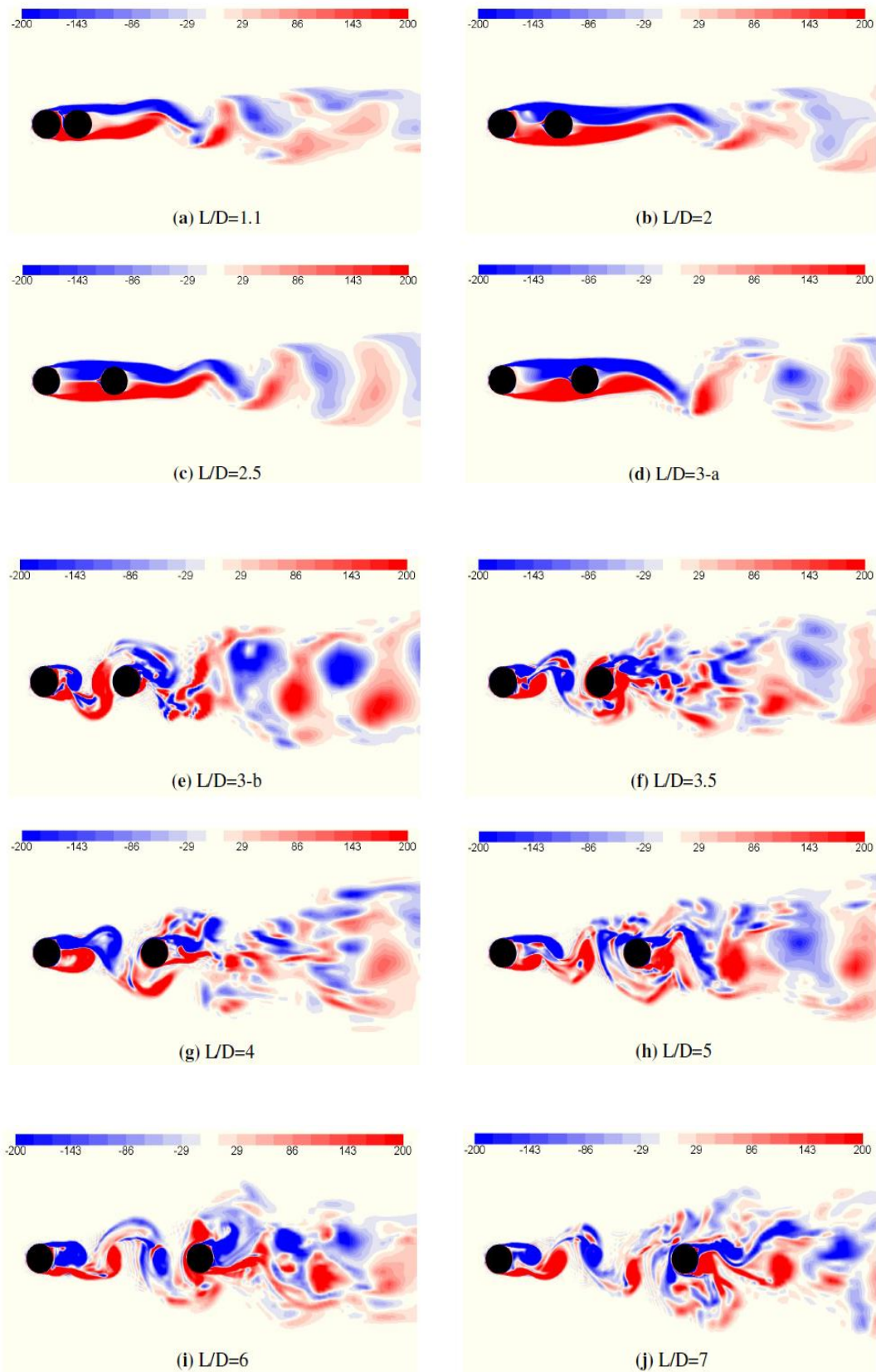
Fig. 7. Instantaneous contours of the z-vorticity field in the mid-span sections for different L/D.

(a) L/D=1.1

(b) L/D=2.5

(c) L/D=5
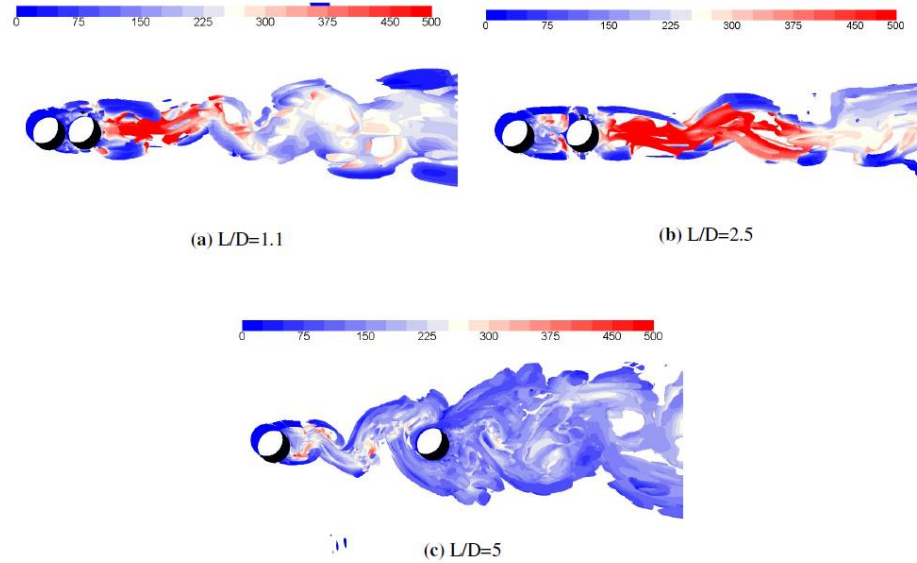
Fig. 8. Iso-surfaces of instantaneous Q-criterion (Q = 1[s−2]) for L/D=1.1, 2.5 and 5.

(a)

(b)
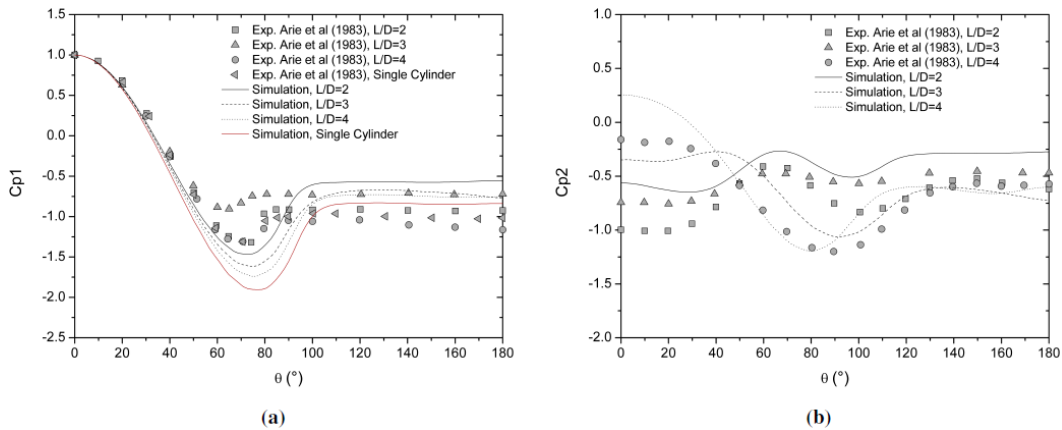
Fig. 9. Time-averaged pressure distributions along the surface of upstream and downstream cylinder: (a) upstream cylinder, (b) downstream cylinder.

surface of the two cylinders at L/D=2, 3 and 4, and on a single cylinder. In the horizontal axes, the symbol θ indicates the angle measured from the front position to the back position of the cylinders in the clockwise direction. Additionally, the experimental results obtained by Arie *et al.* (1983) at Re = 1.57 × 10^5 are plotted in these figures for comparison (the values are represented by solid symbols). As can be seen from the figures, the mean pressure coefficients for the downstream cylinder show a reasonable accuracy regarding the experimental results. Meanwhile, the Cp for the upstream cylinder shows a slightly larger difference with the experiments. These results can be attributed to the fact that the separation point moves to the back side of the cylinder ($\theta s \approx 95 - 100°$). There are no available experimental data to compare the other L/D distances studied in this work. For this reason, Figs. 10 and 11 show the Cp for both the upstream and downstream cylinder, respectively.

From the Figs. 10 and 11, we can describe the flow behavior. For L/D=1.1, there is no sign of the reattachment point, which is because the pressure increases up to a maximum value at the back side of the downstream cylinder ($\theta = 180°$). This behavior indicates that the two cylinders behave as an extended-body because the separate shear layer from the downstream cylinder does not reattach onto the downstream cylinder. For L/D=2 and 2.5, the Cp curve of the downstream cylinder has a similar behavior with a peak value in the pressure distribution for an angle $\theta = 66°$ and $60°$ for L/D=2 and 2.5, respectively. These peaks of Cp correspond to the flow reattachment on the surface of the downstream cylinder (Zdravkovich and Pridden, 1977), and it determines the reattachment regime. The value of θ where the peak value takes place is defined as reattachment angle (θr). Besides, we note that for the upstream cylinder the Cp values for L/D=2 and 2.5 are close between them, and they
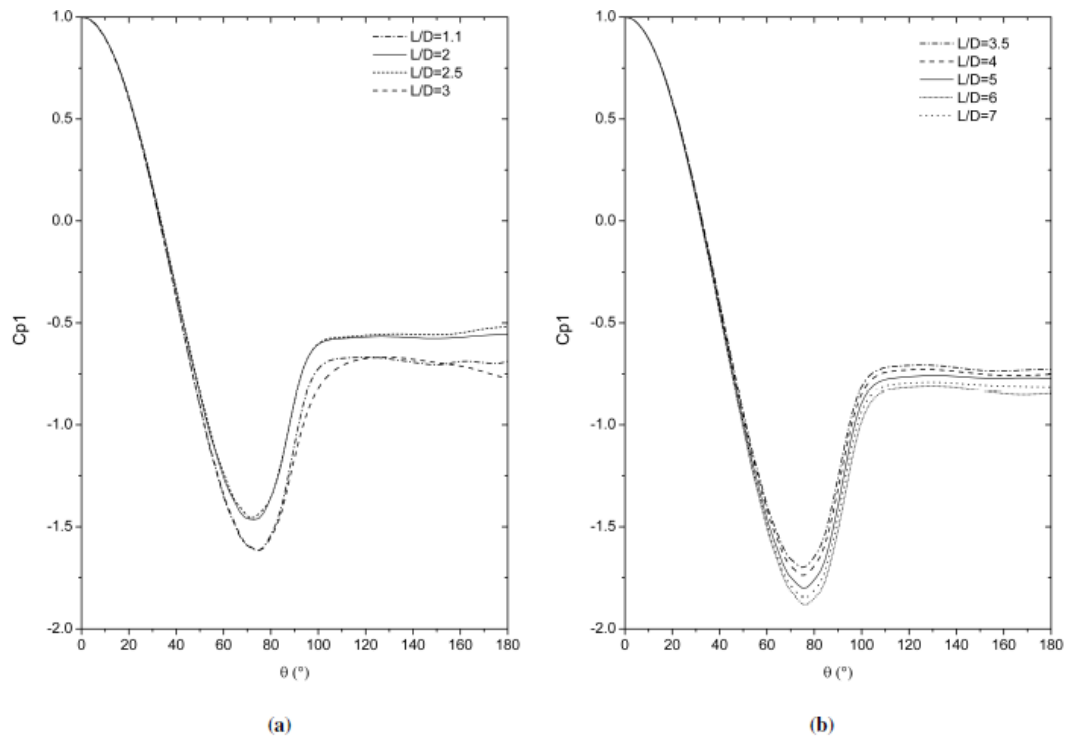
Fig. 10. Time-mean pressure distribution along the surface of upstream cylinder: (a) L/D=1.1, 2, 2.5 and 3; (b) L/D=3.5, 4, 5, 6 and 7.
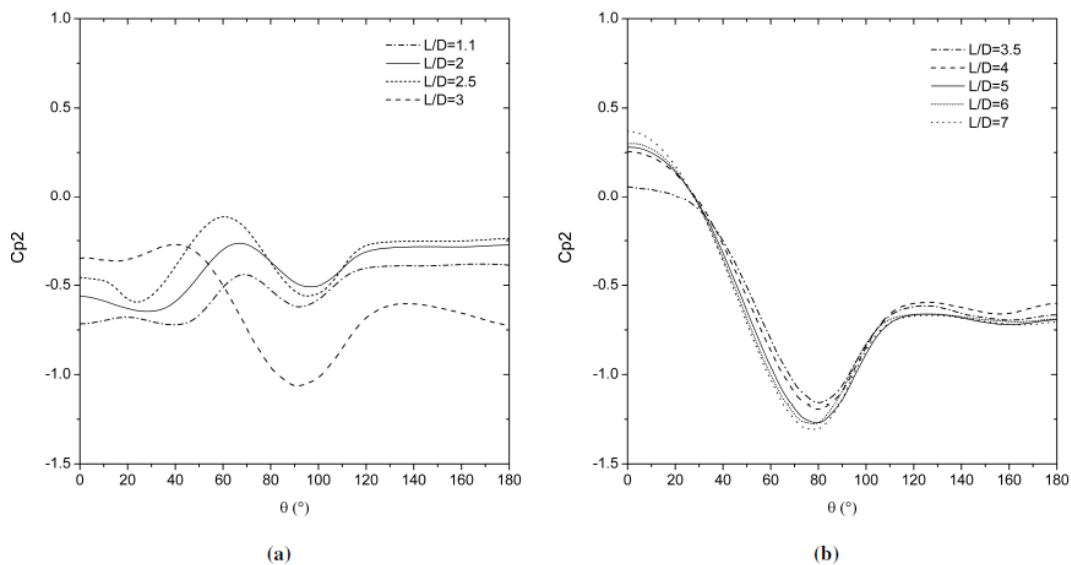
Fig. 11. Time-mean pressure distribution along the surface of downstream cylinder: (a) L/D=1.1, 2, 2.5 and 3; (b) L/D=3.5, 4, 5, 6 and 7.

differ from the other distances. For the critical distance L/D=3, although the downstream cylinder shows a peak in the pressure distribution ($\theta r = 42°$) and the tendency of the Cp curve is similar to the reattachment regime, the pressure values are different, even for the upstream cylinder. For L/D $\geq$ 3.5 the pressure distribution around the downstream cylinder shows a positive pressure close to the front side of the cylinder and the reattachment angle appears at $\theta r = 0°$. The pressure distributions for

L/D $\geq$ 3.5 show a similar curve to the one for a single cylinder. These spacing define the called co-shedding regime.

Fig. 12 shows the Fig angle of the reattachment point (θr) on the downstream cylinder as a function of L/D. The figure shows the results of the experiments conducted for a lower Reynolds number (Re = 1 × 10^4) by Ishigai *et al.* (1972) and a higher Re (Re = 2.1 × 10^5) by Zdravkovich and Pridden (1977) and those obtained in this study.
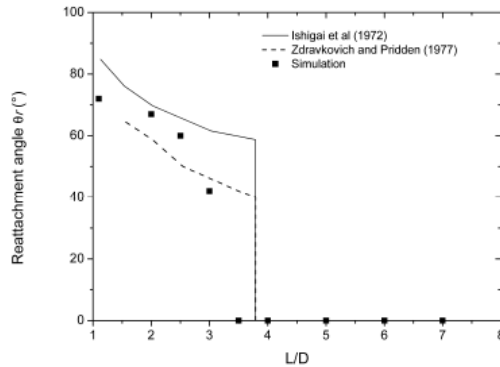
Fig. 12. Positions of the reattachment angle on the downstream cylinder as a function of L/D.

Considering the numerical results obtained for $Re = 1.2 \times 10^5$, we observed a good agreement with experimental data. However, the numerical results deviate slightly from the experiment results near the critical distance, which in this study is found for L/D=3 and in the experiments, the critical spacing ranges from L/D=3.5 to 3.8.

4. CONCLUSION

In this study, numerical simulations employing Scale-Adaptive Simulation (SAS) turbulence model are carried out to study the flow around two circular cylinders of the same diameter arranged in tandem at a high subcritical Reynolds number, $Re = 1.2 \times 10^5$. The interference effects for different nondimensional distances between the cylinders from 1.1 to 7 times the cylinder diameter are analyzed through the values of mean and fluctuating force coefficients, Strouhal number, pressure distribution, as well as through the wake flow structures behind both cylinders. The main conclusions are below.

The mean CD values for the downstream cylinder (CD2) obtained from the present simulations show better accuracy regarding the experimental values. Meanwhile, the mean CD values for the upstream cylinder (CD1) show an underprediction compared with the experiments. For L/D < 3 the downstream cylinder presented a negative drag force, while for L/D > 3 the drag force of the downstream cylinder takes positive values but less than for a single cylinder, even for L/D=7. For the upstream cylinder, the drag coefficient, CLRMS and CDRMS for L/D > 3 showed that the upstream cylinder behaves as an individual entity, i.e., for L/D > 3 the force exerted on the upstream cylinder are not affected by the presence of the downstream cylinder. On the other hand, the critical spacing is obtained for L/D=3, where the time histories of the force coefficients of both cylinders showed two different flow patterns (bistable flow), one pattern momentarily similar to the fluctuating force for the reattachment regime and another pattern similar to the co-shedding regime. The predicted Strouhal number by numerical simulation are in agreement with the experimental data. For L/D ≥ 2.5 the Strouhal number are very similar for both cylinders and when L/D ≥ 5 the Strouhal number approach the value found for a single cylinder. The mean pressure coefficient predicted by numerical simulations shows some differences regarding the experimental data, especially for the upstream cylinder. This behavior is due to the separation point occurs further back from the upstream cylinder when is compared with experiments results. Although some differences are observed in the pressure distribution for the downstream cylinder, the positions of the reattachment angle on this cylinder show a good agreement with experimental data.

These results suggest that the SAS turbulence model can be considered as an alternative to studying the interference effect of blunt bodies often encountered in engineering applications. Note that this model reproduces the experimental data with reasonable agreement.

ACKNOWLEDGMENTS

APPENDIX A. SINGLE CYLINDER

With the objective to compare the behavior of tandem cylinders, numerical simulations for a single cylinder have been performed at $Re = 1.2 \times 10^5$. The computational domain is similar to the tandem cylinders simulations without the domain defined as the spacing L. The boundary conditions employed in this study are the same used by the tan-dem cylinders simulations (see Fig. 1). The mesh resolution and the multi-block structured method are consistent with tandem cylinder meshes with a total number of the grid elements of 0.64 million. This mesh can be seen in Fig. 13(a) and details near the cylinder surface are shown in Fig. 13(b).

The results obtained in the present study are summarized in Table 3. In addition, the mean pressure distribution and the visualization of the wake structure represented by spanwise vorticity, ω_z, in the mid-span sections are given in Figs. 14 and 15, respectively. These results have been used to assess the behavior of a tandem cylinder arrangement in the Results and Discussion section.
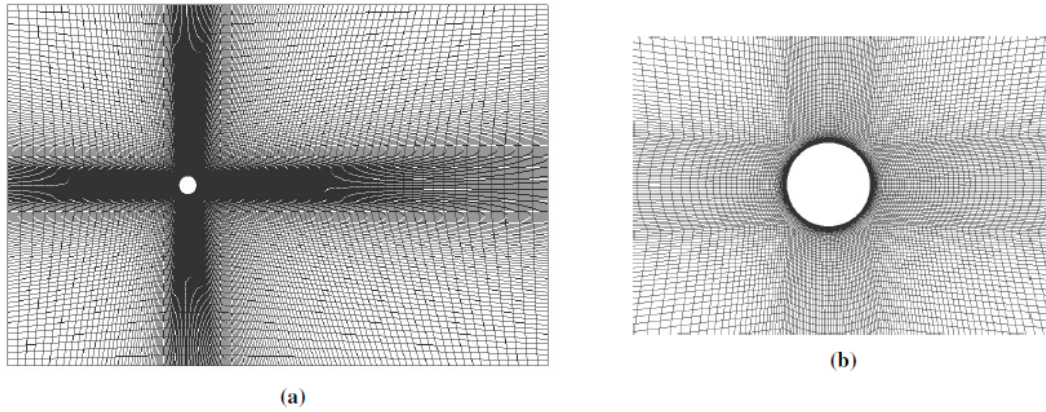
Fig. 13. Mesh used for the single cylinder simulation.
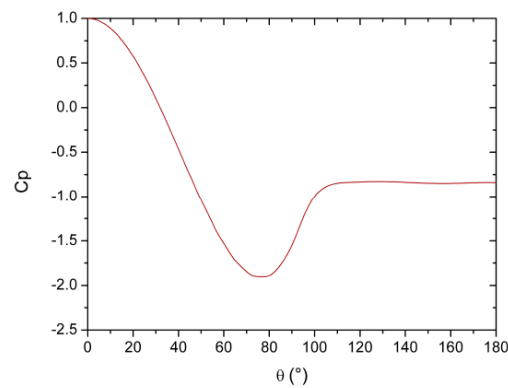
Fig. 14. Pressure distribution for a single cylinder.
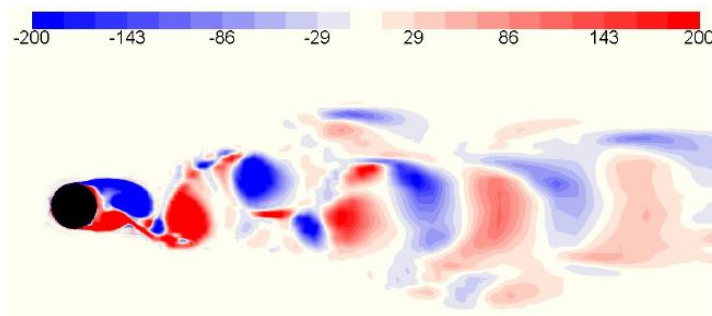
Fig. 15. Wake structure for a single cylinder.

Table 3 Parameter obtained by numerical simulation for a single cylinder

Calculated parameters	Values
Mean drag coefficient	0.730
CL_{RMS}	0.195
CD_{RMS}	0.029
St	0.265

REFERENCES

Alam, M. M. (2014). The aerodynamics of a cylinder submerged in the wake of another. *Journal of Fluids and Structures* 51, 393-400.

Alam, M. M., M. Moriya, K. Takai and H. Sakamoto (2003). Fluctuating fluid forces acting on two circular cylinders in a tandem arrangement at a subcritical reynolds number. *Journal of Wind Engineering and Industrial Aerodynamics* 91(1-2), 139-154.

Ansys-Fluent (2014). 15.0 user's guide. Ansys Inc.

Ansys-ICEM (2014). 15.0 user's guide. Ansys Inc.

Arie, M., M. Kiya, M. Moriya and H. Mori (1983). Pressure fluctuations on the surface of two circular cylinders in tandem arrangement. *Journal of fluids engineering* 105(2), 161-166.

Biermann, D. and W. H. Herrnstein Jr (1934). The interference between struts in various combinations. In *National Advisory Committee For Aeronautics*, 3-13.

Carmo, B. and J. Meneghini (2006). Numerical investigation of the flow around two circular cylinders in tandem. Journal of Fluids and Structures 22(6-7), 979–988.

Dobrucali, E. and O. Kinaci (2017). Urans-based prediction of vortex induced vibrations of circular cylinders. *Journal of Applied Fluid Mechanics* 10(3), 957-970.

Grioni, M., S. Elaskar, and A. Mirasso (2018). Scale-adaptive simulation of flow around a circular cylinder near a plane boundary. *Journal of Applied Fluid Mechanics* 11(6), 1477–1488.

Igarashi, T. (1981). Characteristics of the flow around two circular cylinders arranged in tandem: 1st report. *Bulletin of JSME* 24(188), 323–331.

Igarashi, T. (1984). Characteristics of the flow around two circular cylinders arranged in tandem: 2nd report, unique phenomenon at small spacing. *Bulletin of JSME* 27(233), 2380-2387.

Ishigai, S., E. Nishikawa, K. Nishimura and K. Cho (1972). Experimental study on structure of gas flow in tube banks with tube axes normal to flow: Part 1, karman vortex flow from two tubes at various spacings. *Bulletin of JSME* 15(86), 949-956.

Jendrzejczyk, J. and S. Chen (1985). *Fluid forces on two circular cylinders in crossflow*. Technical report, Argonne National Lab., IL (USA).

Kitagawa, T. and H. Ohta (2008). Numerical investigation on flow around circular cylinders in tandem arrangement at a subcritical reynolds number. *Journal of Fluids and Structures* 24(5), 680-699.

Liang, C., G. Papadakis, and X. Luo (2009). Effect of tube spacing on the vortex shedding characteristics of laminar flow past an inline tube array: a numerical study. *Computers & Fluids* 38(4), 950-964.

Ljungkrona, L., C. Norberg, and B. Sunden (1991). Free-stream turbulence and tube spacing effects on surface pressure fluctuations for two tubes in an in-line arrangement. *Journal of Fluids and Structures* 5(6), 701-727.

Meneghini, J. R., F. Saltara, C. Siqueira and J. Ferrari Jr (2001). Numerical simulation of flow interference between two circular cylinders in tandem and side-by-side arrangements. *Journal of fluids and structures* 15(2), 327-350.

Menter, F. R. (1994). Two-equation eddy- viscosity turbulence models for engineering applications. *AIAA journal* 32(8), 1598–1605.

Menter, F., M. Kuntz and R. Bender (2003). A scale-adaptive simulation model for turbulent flow predictions. In *41st aerospace sciences meeting and exhibit*, 767.

Mittal, S., V. Kumar, and A. Raghuvanshi (1997). Unsteady incompressible flows past two cylinders in tandem and staggered arrangements. *International Journal for Numerical Methods in Fluids* 25(11), 1315-1344.

Niemann, H. J. and N. Hölscher (1990). A review of recent experiments on the flow past circular cylinders. *Journal of Wind Engineering and Industrial Aerodynamics* 33(1-2), 197–209.

Okajima, A. (1979). Flows around two tandem circular cylinders at very high reynolds numbers. *Bulletin of JSME* 22(166), 504-511.

Palau-Salvador, G., T. Stoesser and W. Rodi (2008). LES of the flow around two cylinders in tandem. *Journal of Fluids and Structures* 24(8), 1304-1312.

Rajani, B., A. Kandasamy and S. Majumdar (2012). On the reliability of eddy viscosity based turbulence models in predicting turbulent flow past a circular cylinder using URANS approach. *Journal of Applied Fluid Mechanics* 5(11), 67-79.

Sumner, D. (2010). Two circular cylinders in cross-flow: a review. *Journal of Fluids and Structures* 26(6), 849-899.

Wang, L., M. M. Alam and Y. Zhou (2018). Two tandem cylinders of different diameters in cross-flow: Effect of an upstream cylinder on wake dynamics. *Journal of Fluid Mechanics* 836, 5-42.

Zdravkovich, M. (1987). The effects of interference between circular cylinders in cross flow. *Journal of fluids and structures* 1(2), 239-261.

Zdravkovich, M. and D. Pridden (1977). Interference between two circular cylinders; series of unexpected discontinuities. *Journal of wind engineering and industrial aerodynamics* 2(3), 255-270.

Zhang, H. and W. Melbourne (1992). Interference between two circular cylinders in tandem in turbulent flow. *Journal of Wind Engineering and Industrial Aerodynamics* 41(1-3), 589-600.